RSC Advances

PAPER

View Article Online
View Journal | View Issue

Cite this: *RSC Adv.*, 2023, **13**, 36373

Effect of calcium ion concentration on the ORR performance of Pd/C catalysts†

Lin jun Tong,[a] Xiaojuan Lin,[a] Jian wen Cai,[a] Wen Fu[b] and Xiaoting Deng *[c]

Noble metal electrocatalysts prepared by microbial methods have attracted extensive attention because of their environmental protection and easy preparation. However, the preparation of electrocatalysts by microbial methods has problems such as large nanoparticles size and low loading rate. In this study, the porous gel co-embedded with *Shewanella* and alginate is prepared as the adsorption matrix to further enhance its mass transfer and adsorption efficiency. The effect of calcium ion concentration on catalyst performance is explored by optimizing the $CaCl_2$ concentration to expose more adsorption sites. The results show that when the Ca^{2+} concentration is 0.025 mmol L^{-1}, the prepared catalyst has the smallest size and the highest Pd loading, and exhibits the best electrochemical activity and stability. This provides a new idea for the preparation of electrocatalysts by microbial methods.

Received 5th November 2023
Accepted 7th December 2023

DOI: 10.1039/d3ra07553b

rsc.li/rsc-advances

1. Introduction

Proton exchange membrane fuel cells are widely studied due to their advantages of fast start-up and zero emissions. The development of commercial Pt-based catalysts is severely restricted due to the low reserves of Pt.[1] As a main group element of Pt, Pd has similar chemical properties to Pt.[2] Therefore, Pd-based catalysts have also been widely studied. At present, the main methods for the synthesis of electrocatalysts include physical, chemical and biological methods. Among the many synthesis methods, microbial synthesis has received widespread attention.[3]

The microbial synthesis method is a method of *in situ*, clean and mild synthesis of nano-metals by utilizing the good adsorption and reducing power of microorganisms on metals. The research on microbial synthesis of nanomaterials can be traced back to the use of *Candida glabrata* to synthesize intracellular CdSe nanomaterials in 1989,[4] and the biosynthesis of *Fusarium oxysporum* was used in 2001 Ag nanoparticles, the first successful proof-of-concept biosynthetic technology.[5] During the microbial synthesis of nanomaterials, there are a wide range of factors affecting the performance of nanomaterials, mainly including microbial characteristics (such as the type of microorganism, age of microbial inoculation and type of growth medium) and process conditions (such as pH value and temperature), and process kinetics of interactions between metal ion precursors and reducing agents, adsorption kinetics of stabilizers and nanoparticles.[6]

Shewanella is a Gram-negative and anaerobic bacterium.[7] It is a typical dissimilatory metal-reducing bacteria. It is widely distributed in various natural and artificial environments. More than 50 species have been isolated and identified. *Shewanella* possesses a complex multi-set branched-chain electron transport system that facilitates the reduction of different terminal electron acceptors, which includes inner membrane-localized dehydrogenases, methaqualone, and various cytochromes. At present, in terms of reducing metals, it has been confirmed that *Shewanella* can reduce Fe(III), Mn(IV), Cr(VI), Np(V), Tc(VII), Pu(IV), V(V), Se(IV), Te(IV), Au(III), Ag(I), Pd(II) and Cu(II), *etc.*[7–9]

However, traditional microbial reduction easily leads to the agglomeration of nanoparticles and low metal utilization.[11] Microbe embedding filling refers to blending microorganisms with sodium alginate, and then cross-linking to prepare a gel, so as to improve the performance of the composite gel and effectively reduce the size of nanoparticles. A number of studies have shown that the material modified by embedding and filling can have both the advantages of gel and filling material.[12] On the one hand, it avoids the problems of easy loss and difficult recycling of fine filling materials. On the other hand, the blended filling enhances its adsorption performance and environmental adaptability.

In this study, *Shewanella oneidensis* MR-1, calcium alginate and calcium carbonate were used as the composite adsorption matrix, and by reducing the concentration of calcium alginate in the adsorption matrix, fully exposing its carboxyl, hydroxyl and other oxygen-containing functional groups, so as to further improve the palladium loading of calcium alginate–calcium carbonate porous composite carbon matrix catalysts.

[a]*FoShan Poly Technic, Foshan, 528000, China*
[b]*Guangdong Hydrogen Engine New Material Co., Ltd, Foshan, 528000, China*
[c]*College of Food and Chemical Engineering, Shaoyang University, Shaoyang 422000, China. E-mail: Xiaotingdeng@126.com*

† Electronic supplementary information (ESI) available. See DOI: https://doi.org/10.1039/d3ra07553b

2. Experimental part

2.1 Chemicals

The bacterial seeds of *Shewanella oneidensis* MR-1 (99%) were purchased from American Type Culture Collection. Sodium tetrachloropalladate (Na_2PdCl_4), calcium chloride ($CaCl_2$), sodium alginate, disodium hydrogen phosphate (Na_2HPO_4), calcium carbonate ($CaCO_3$), and Nafion (5 wt%) were purchased from Sinopharm Chemical Reagent Co., Ltd. All the reagents and solvents were used without further purification. Commercial 10% Pd/C was obtained from Johnson Matthey Company. DI water (18.2 MΩ × cm) was produced in our laboratory.

2.2 Synthesis of catalysts

2.2.1 *Shewanella oneidensis* MR-1 activation expansion. *Shewanella oneidensis* MR-1 was taken out from the −80 °C refrigerator, streaked on LB solid medium, and incubated at 30 °C for 20 h. Picking a single colony and inoculating it in 100 ml LB liquid medium, culturing it on a shaker at 180 rpm at 30 °C for 18 hours, then inoculate the activated bacterial solution into 1500 ml LB liquid medium according to the inoculum size of 5%, shake it at 180 rpm at 30 °C bed culture for 15 h. The expanded cultured bacteria were collected by centrifugation and washed with sterilized phosphate buffer and deionized water.

2.2.2 Preparation of compound gel adsorption matrix. Preparation of gels adsorption matrix with three different calcium ion concentration, the specific preparation process was as follows: the collected bacteria were added to an aqueous solution containing sodium alginate 2 wt% and calcium carbonate 1.5 wt%. The mixture was then dropped into 100 ml of $CaCl_2$ solution with different concentration. After 2 h of crosslinking, the gel ball was formed. Taking out the gel balls and place them in 0.2 mol per L HCl solution for 20 minutes to make pores. After the gel balls float up, it means that $CaCO_3$ has successfully made pores. The composite gel adsorption matrix co-embedded with MR1 and calcium alginate was obtained.

The concentration of $CaCl_2$ is 0.05 mmol L^{-1}, 0.025 mmol L^{-1} and 0.0125 mmol L^{-1}, respectively. And the composite gel adsorption matrix were labeled as $GAM_{0.05}$, $GAM_{0.025}$ and $GAM_{0.0125}$ correspondingly.

2.2.3 Synthesis of $Pd/C_{0.05}$, $Pd/C_{0.025}$ and $Pd/C_{0.0125}$. $GAM_{0.05}$, $GAM_{0.025}$ and $GAM_{0.0125}$ adsorption matrices were prepared into gel balls, placed in 25 ml of deionized water, and adjusted pH = 3 with HCl. In addition, 3 parts of 75 ml sodium tetrachloropalladate solution with a concentration of 6.89 mmol L^{-1} and pH = 3 were prepared. Sodium tetrachloropalladate solution was dropped into the above three adsorption substrates at a rate of 0.5 ml min^{-1} using a peristaltic pump, and stirred with a magnetic stirrer for 24 h.

The three samples completed by adsorption were freeze-dried in a vacuum overnight. After drying, the sample is placed in a tube furnace and annealed at 800 °C for 3 h in argon atmosphere at a heating rate of 3 °C min^{-1}. Then a reduction process was conducted at 200 °C in H_2 atmosphere for 2 h, the palladium carbon catalyst product was obtained. The samples obtained were named as $Pd/C_{0.05}$, $Pd/C_{0.025}$ and $Pd/C_{0.0125}$, respectively. The inductively coupled plasma (ICP) results show that the Pt content in $Pd/C_{0.05}$, $Pd/C_{0.025}$ and $Pd/C_{0.0125}$ is 9.56%, 10.38%, and 7.64%. In addition, the N contents in $Pd/C_{0.05}$, $Pd/C_{0.025}$ and $Pd/C_{0.0125}$ are 5.0%, 5.2% and 4.9% respectively.

2.3 Physicochemical and electrochemical characterization

The physicochemical and electrochemical characterization details are presented in the ESI.†

3. Results and discussion

3.1 Structural characterization

Fig. 1 shows the SEM images of $Pd/C_{0.05}$, $Pd/C_{0.025}$ and $Pd/C_{0.0125}$. All the prepared catalysts have a porous structure, and there are many pits with uniform size distribution on the surface of the material, which is beneficial to the loading of Pd nanoparticles. By comparing the morphology images of $Pd/C_{0.05}$ and $Pd/C_{0.025}$, it was found that with the Ca^{2+} concentration decreases, the gel cross-linking degree decreases, and the pores of the carbon carrier in $Pd/C_{0.025}$ become larger. However, when the concentration of Ca^{2+} is further reduced, the pore-forming effect of $CaCO_3$ is not obvious because the gel cross-linking is too low and weak. In addition, in order to further determine the specific surface area of the catalyst, the BET test was conducted on the catalyst. As shown in Fig. S1,† the specific surface areas of $Pd/C_{0.05}$, $Pd/C_{0.025}$ and $Pd/C_{0.0125}$ were 40.95 $m^2 g^{-1}$, 44.56 $m^2 g^{-1}$ and 13.05 $m^2 g^{-1}$.

The morphology and particle size of as-prepared catalyst are shown in Fig. 2. The size distribution of Pd nanoparticles was obtained by randomly measuring the sizes of 150 nanoparticles from the SEM images. It is particularly noticeable that the average particle size of $Pd/C_{0.05}$ and $Pd/C_{0.025}$ was significantly smaller than that of $Pd/C_{0.0125}$, and the average particle size was 8.34 nm, 7.84 nm and 16.21 nm, respectively. The conditions of the as-prepared catalysts are the same except for the concentration of $CaCl_2$, so it can be concluded that the degree of crosslinking of $CaCl_2$ has a great influence on the distribution of metals. When the Ca^{2+} concentration is 0.0125 mM, the PdNPs formed are the largest, because the formed gel has weak coagulation and fixation ability, and calcium alginate cannot fix microorganisms in a limited space, so the cells will contact and agglomeration of palladium ions occurs during the reduction. However, when the Ca^{2+} concentration is 0.025 mM and 0.05 mM, the particle size distribution of PdNPs is relatively small, both of which are about 8 nm, indicating that the higher Ca^{2+} concentration range will not affect the size of palladium particles. Therefore, the size of nano-palladium will not be affected within a certain range of cross-linking degree, but too low cross-linking will affect the immobilization effect of the gel on microorganisms. The metal particles of the prepared palladium carbon catalyst become larger. The spacing of the lattice fringe shown in Fig. 2(b), (e) and (h) was 0.224 nm, corresponding to the (111) plane of Pd face centered cubic.[13]

Fig. 3a illustrates the XRD patterns of $Pd/C_{0.05}$, $Pd/C_{0.025}$ and $Pd/C_{0.0125}$. The XRD curve has a obvious diffraction peak at 40.2° and 46.62°, corresponding to the (111) and (220) crystal face of

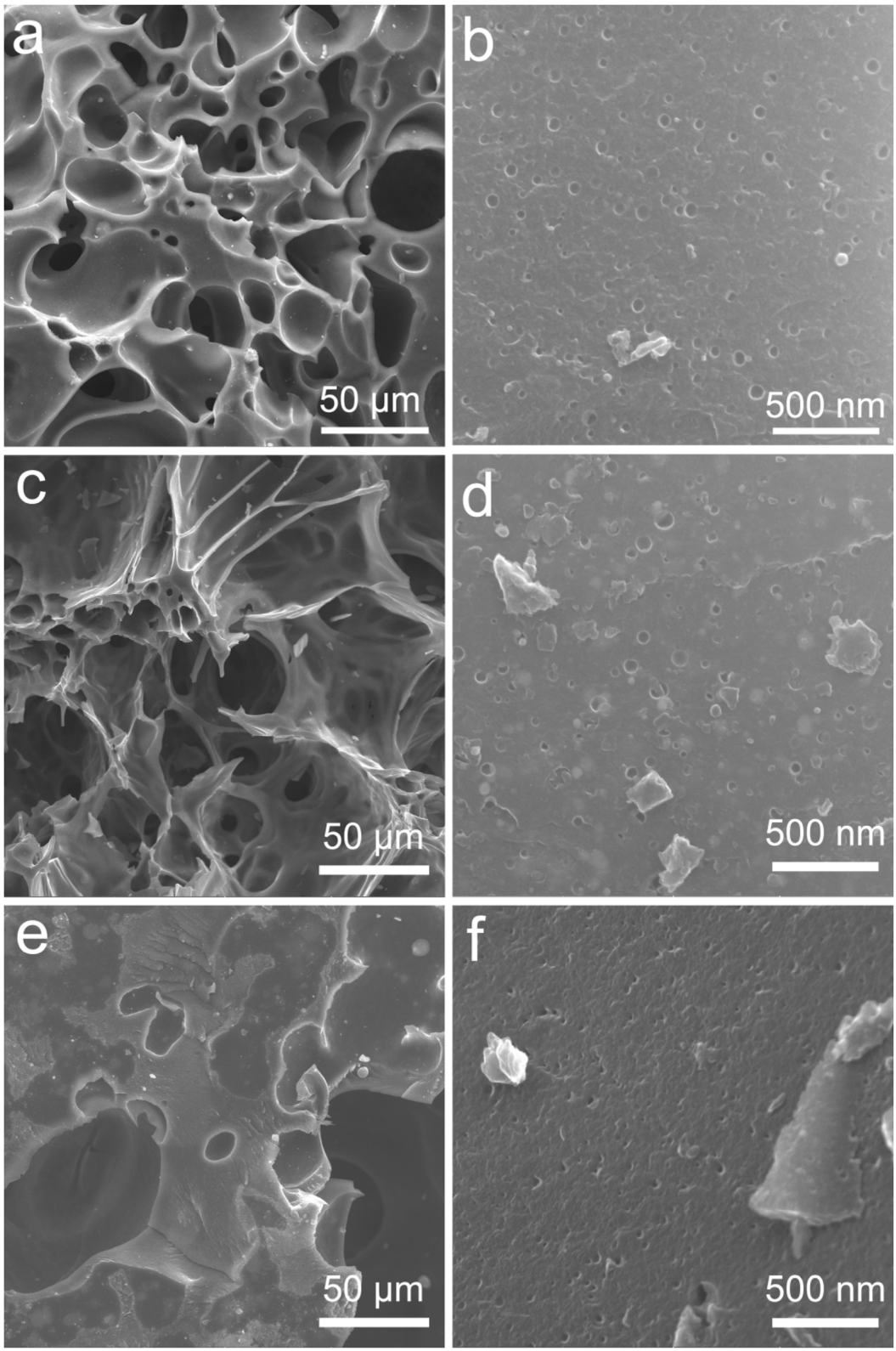

Fig. 1 SEM images of the (a and b) Pd/$C_{0.05}$, (c and d) Pd/$C_{0.025}$ and (e and f) Pd/$C_{0.0125}$.

Pd, respectively.[8] In this study, the amount of Ca^{2+} was changed, but there was no significant difference in the crystal structure, which indicated that Ca^{2+} had little effect on the Pd crystal.

The Raman results of Pd/C catalysts prepared with different concentrations of Ca^{2+} are shown in Fig. 3b. The I_D/I_G ratios of Pd/$C_{0.05}$, Pd/$C_{0.025}$ and Pd/$C_{0.0125}$ are 0.92, 0.89 and 0.87

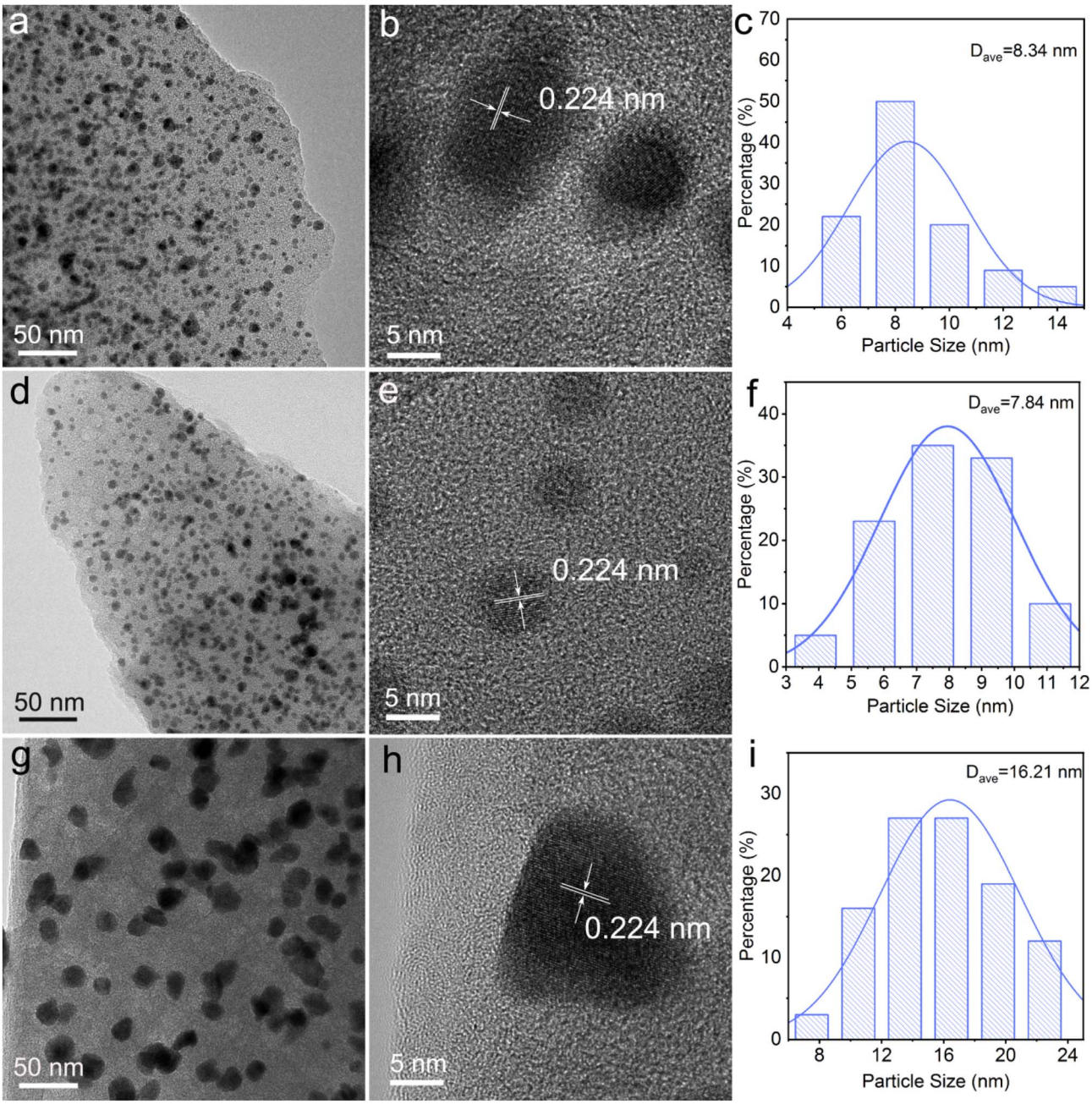

Fig. 2 TEM images and Pd size distribution of the (a–c) Pd/$C_{0.05}$, (d–f) Pd/$C_{0.025}$ and (g–i) Pd/$C_{0.0125}$.

respectively. This result shows that with the decrease of Ca^{2+} concentration, the I_D/I_G ratio shows a downward trend. It can be further concluded that the degree of graphitization increases with the decrease of Ca^{2+} concentration.

To investigate the electronic structure of Pd in as-prepared catalyst were characterized by XPS measurements. Each Pd 3d XPS spectrum of Pd/$C_{0.05}$, Pd/$C_{0.025}$ and Pd/$C_{0.0125}$ were decomposed into Pd^0 peak and Pd^{2+} peak according to the binding energy. As shown in Fig. 4a and Table 1, the content of Pd(0) decreases with the decrease of Ca^{2+} concentration, indicating that the degree of cross-linking of Ca^{2+} has an effect on the palladium reduction process. This may be due to the porous structure of the carbon matrix. The porous structure has a more efficient mass transfer channel and an increased contact area of H_2, so the reduction rate of the phase is slightly improved. Generally, different kinds of nitrogen play different functions. For example, graphitic nitrogen has weak electron donating ability and contributes less to the ORR, but it can improve the conductivity of the carbon matrix. The lone pair of electrons in pyridine nitrogen endows it with electron-donating ability, which can effectively provide Lewis base sites, and the ORR performance of carbon catalysts with high pyridine nitrogen doping is better. In addition, pyrrole nitrogen is extremely unstable and prone to various

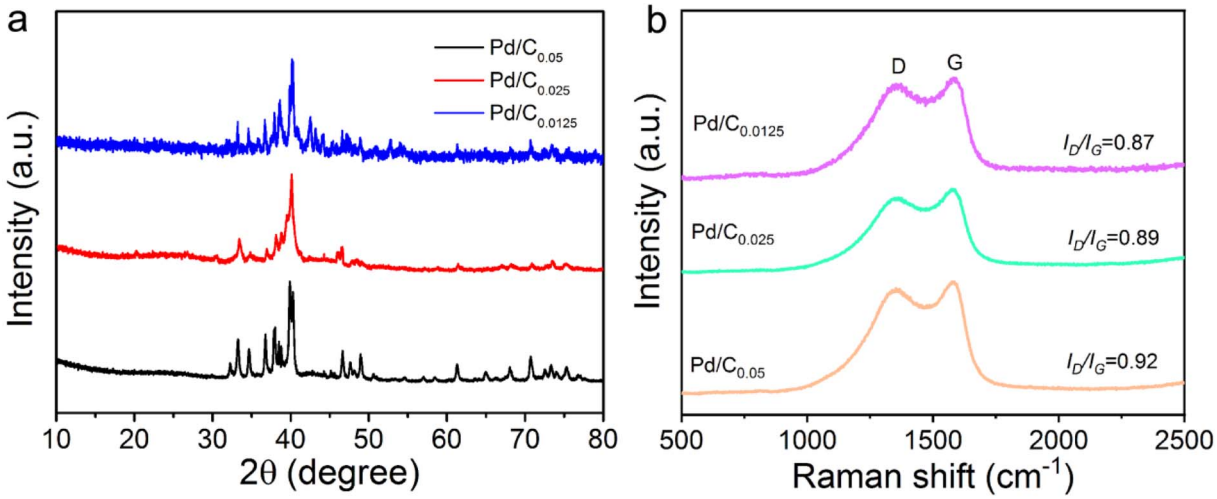

Fig. 3 (a) XRD spectra patterns and (b) Raman of $Pd/C_{0.05}$, $Pd/C_{0.025}$ and $Pd/C_{0.0125}$, respectively.

transformations. In our previous research, we found that different carbon substrates will affect the nitrogen species of the catalyst, and alginate is more likely to generate pyridinic nitrogen. As shown in Fig. 4b and Table 1, since all samples in the three groups of samples use calcium alginate composite carbon matrix, the proportion of pyridine nitrogen in the obtained samples is large (about 38%), which promotes the better performance of the catalyst. In addition, the graphitic N content increases with decreasing Ca^{2+} concentration, which corresponds to the increase in graphitization degree with decreasing Ca^{2+} concentration.

3.2 Electrocatalytic activity for ORR

The LSV curve and electron transfer number are shown in Fig. 5, and the calculation results of the electrochemical activity index are shown in Table 2. Limiting current density and half-wave potential are important indicators for judging catalyst activity,

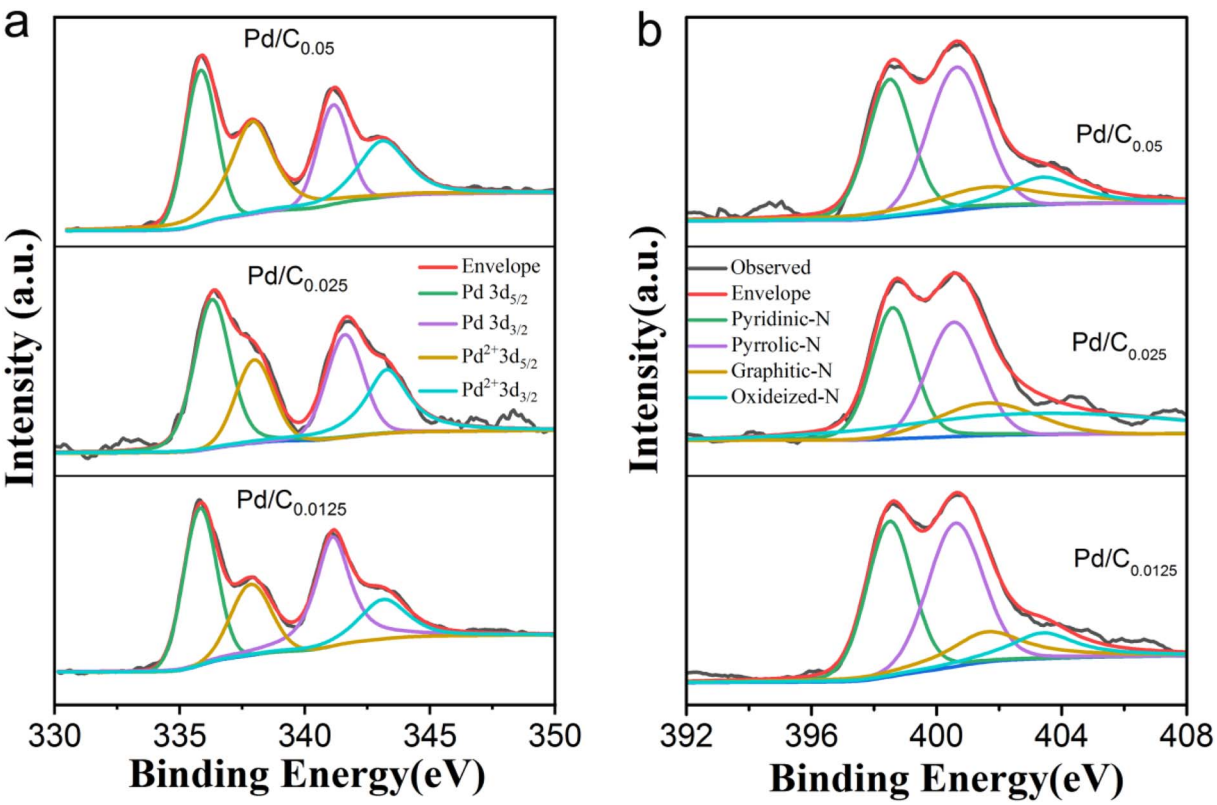

Fig. 4 (a) Pd 3d spectra and (b) N 1S spectra of $Pd/C_{0.05}$, $Pd/C_{0.025}$ and $Pd/C_{0.0125}$, respectively.

Table 1 Types and content of Pd and N in $Pd/C_{0.05}$, $Pd/C_{0.025}$ and $Pd/C_{0.0125}$ catalysts with different Ca^{2+} concentration

Sample	Pd(0)	Pd(II)	Pyridinic-N	Pyrrolic-N	Graphitic N	Oxidized-N
$Pd/C_{0.05}$	60.32%	39.68%	39.88%	38.72%	17.75%	3.65%
$Pd/C_{0.025}$	58.45%	41.55%	38.72%	36.45%	20.08%	4.75%
$Pd/C_{0.0125}$	47.85%	52.15%	37.43%	36.41%	21.76%	4.40%

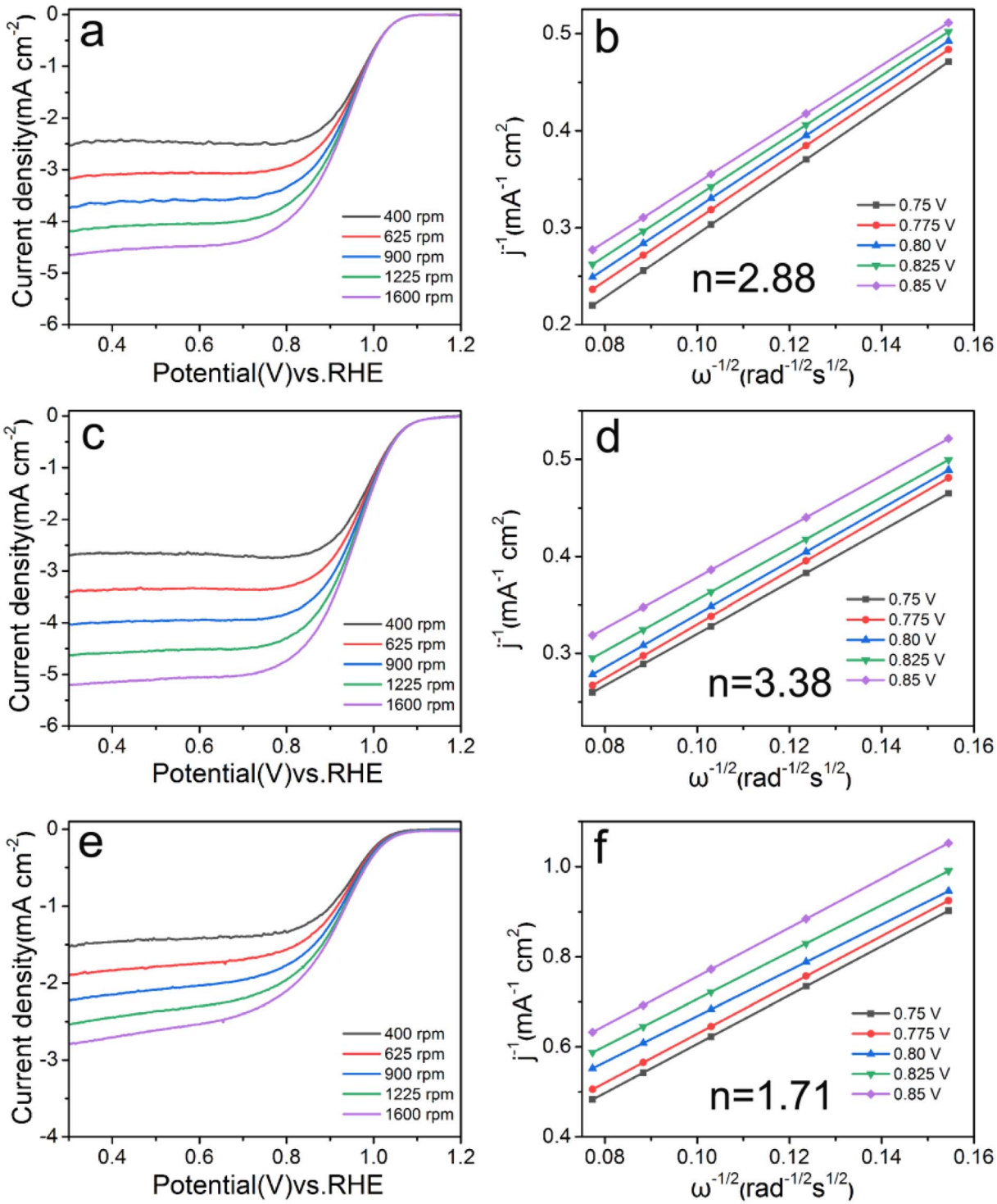

Fig. 5 LSV and Koutecky–Levich plots of (a and b) $Pd/C_{0.05}$, (c and d) $Pd/C_{0.025}$ and (e and f) $Pd/C_{0.0125}$ at 0.75–0.85 V, respectively.

Table 2 Electrochemical activity indices of as-prepared samples and commercial Pd/C

Sample	$E_{1/2}$ (V)	ECSA ($m^2\ g^{-1}$)	MA ($A\ mg^{-1}$)	SA ($A\ m^{-2}$)	Pd (wt%)
$Pd/C_{0.05}$	0.929	26.35	0.22	0.84	9.56
$Pd/C_{0.025}$	0.952	47.05	0.37	0.79	10.38
$Pd/C_{0.0125}$	0.905	34.29	0.10	0.29	7.64
Commercial Pd/C	0.786	26.97	0.08	0.31	9.89

and it is generally believed that the larger of the value, the better the electrochemical catalytic effect.[14] With the concentration of Ca^{2+} from 0.05 mM to 0.025 mM, the values of these two index parameters are all increasing, indicating that reducing the Ca^{2+} concentration is beneficial to the catalytic reaction. When the concentration was too low (0.0125 mM), the half-wave potential of $Pd/C_{0.0125}$ (0.905 V) were significantly lower than those of $Pd/C_{0.05}$ (0.929 V), $Pd/C_{0.025}$ (0.952 V).

As shown in Fig. 5 and S2,† $Pd/C_{0.05}$, $Pd/C_{0.025}$, $Pd/C_{0.0125}$ and Pd/C were calculated by the Koutecky–Levich equation at 0.75 V, 0.775 V, 0.80 V, 0.825 V and 0.85 V, the corresponding average electron transfer numbers are 2.88, 3.38, 1.71 and 2.26, respectively. With the decrease of calcium ion concentration, the number of electron transfer first increased and then decreased. The $Pd/C_{0.025}$ catalyst follows the four-electron reaction pathways and the two-electron reaction pathways occurring simultaneously, while the $Pd/C_{0.0125}$ follows the two-electron reaction pathway. This indicates that the Ca^{2+} concentration of 0.025 mM is the most suitable for the catalytic reaction.

The CV test results of different catalyst samples are shown in Fig. 6. It can be seen that the catalysts with the Ca^{2+} concentration of 0.05 mM and 0.025 mM have obvious oxygen reduction peaks, but the oxygen reduction peak is not obvious when

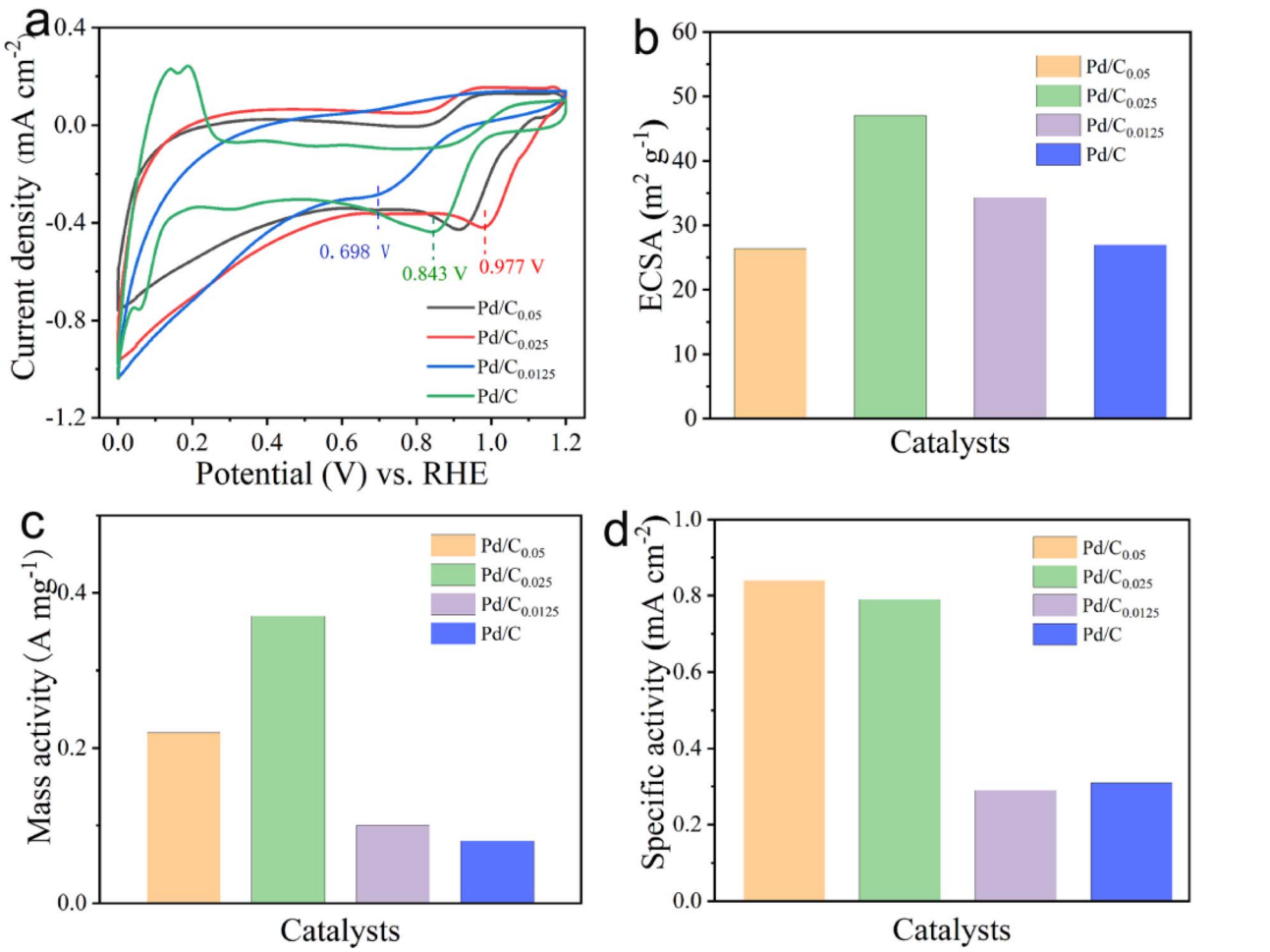

Fig. 6 (a) CV, (b) ECSA (c) MA and (d) SA of $Pd/C_{0.05}$, $Pd/C_{0.025}$ and $Pd/C_{0.0125}$ in 0.1 M KOH solution with potential scanning rate of 10 mV s^{-1} respectively.

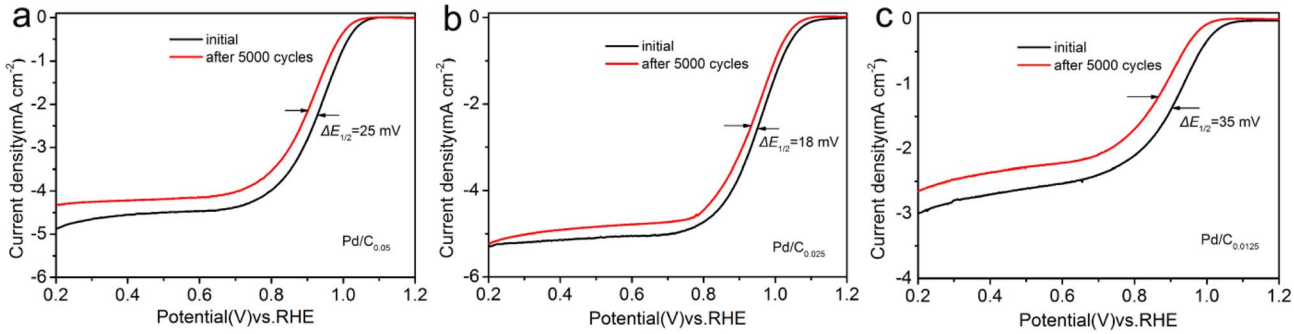

Fig. 7 LSV curves of (a) Pd/$C_{0.05}$, (b) Pd/$C_{0.025}$ and (c) Pd/$C_{0.0125}$ before and after 5000 potential cycles.

the Ca^{2+} concentration is reduced to 0.0125 mM. It can be seen from the figure that the oxygen reduction peak sites of Pd/$C_{0.05}$, Pd/$C_{0.025}$, Pd/$C_{0.0125}$ and Pd/C appeared respectively at 0.914 V, 0.977 V, 0.698 V and 0.843 V. The more positive the peak potential, the easier it is for O_2 to be reduced and the better the catalyst effect. Combined with the previous data, it can be seen that the oxygen reduction peak site is gradually shifting positively after reducing the Ca^{2+} concentration, implying that the catalyst can exert better electrochemical performance. However, it is worth noting that the oxygen reduction peak of Pd/$C_{0.0125}$ becomes indistinct and the current density is extremely small. It shows that reducing the concentration of calcium in an appropriate concentration range can improve the performance of the catalyst, but too low concentration will make the catalytic effect worse.

The electrochemical surface area (ECSA) is an important indicator for evaluating the active sites of catalysts. As shown in Fig. 6b, The calculated ECSAs are 26.35, 47.05, 34.29 and 26.97 $m^2\ g^{-1}$ for Pd/$C_{0.05}$, Pd/$C_{0.025}$, Pd/$C_{0.0125}$ and Pd/C, respectively. Obviously, calcium ion concentration has certain influence on ECSA. This result suggests that more active sites exist in Pd/$C_{0.025}$, which can be attributed primarily to the size of Pd NPs and Pd load.

In addition, MA and SA are important indicators for evaluating catalyst performance. The kinetic current density (j_k), mass activity (MA) and specific activities (SA) can be calculated by the following equation:

$$1/j = 1/j_k + 1/j_d$$

where j is the measured current density and j_d is the measured limiting current.

$$MA = j_k/Pd_{load}$$

$$SA = MA/ECSA^{15}$$

As shown in Fig. 6(c) and (d), the MA of Pd/$C_{0.025}$ is 0.37 A mg^{-1}, which was 3.7 times higher than that of Pd/$C_{0.0125}$ (0.10 A mg^{-1}). The SA of Pd/$C_{0.05}$, Pd/$C_{0.025}$ and Pd/$C_{0.0125}$ is 0.84 mA cm^{-2}, 0.79 mA cm^{-2} and 0.29 mA cm^{-2}, respectively. Above all, Pd/$C_{0.0125}$ has the best oxygen reduction performance. This is due to the small and uniform particle distribution of Pd/$C_{0.0125}$.

Accelerated stability testing was used to evaluate the stability performance of the catalyst. Comparing the LSV curves before and after ADT (Fig. 7), it is found that $E_{1/2}$ negatively shifted by 25 mV and 35 mV for Pd/$C_{0.05}$ and Pd/$C_{0.0125}$, respectively, whereas that of Pd/$C_{0.025}$ only decreased 18 mV. These results confirmed that Pd/$C_{0.025}$ have excellent stability for ORR in alkaline media.

4. Conclusion

In this study, calcium alginate and *Shewanella oneidensis* MR-1 were used as the composite matrix, and $CaCO_3$ was used as the pore-forming agent to prepare a porous composite Pd/C catalyst. The influence of different concentration of calcium alginate on the performance of the catalyst was explored. The research results show that the average particle size of Pd catalysts with $CaCl_2$ concentration of 0.05 mM, 0.025 mM and 0.0125 mM are 8.34 nm, 7.84 nm and 16.21 nm respectively. This is due to the weak fixation ability of the gel formed by low cross-linking (0.0125 mM), and alginate cannot fix microorganisms in a limited space, so the cells will contact and agglomerate palladium during the reduction process. Electrochemical results show that in the appropriate concentration range, the performance of the catalyst further increases with the decrease of Ca^{2+} concentration, and the optimum concentration is 0.025 mM. However, when the cross-linking is too low (Pd/$C_{0.0125}$), the catalytic effect is even worse. This may be due to the larger palladium particles formed under this condition, and the better performance of Pd/$C_{0.025}$ is due to the increase in palladium loading (10.38%).

Conflicts of interest

There are no conflicts to declare.

Acknowledgements

This paper was supported by funding from Guangdong Province Vocational College Hydrogen Energy Vehicle Industry Education Integration Innovation Platform (2021CJPT024) and Foshan Science and Technology Innovation Project (1920001004360).

References

1 Y. Mo, S. Feng, T. Yu, J. Chen, G. Qian, L. Luo and S. Yin, Surface unsaturated WOx activating PtNi alloy nanowires for oxygen reduction reaction, *J. Colloid Interface Sci.*, 2022, **607**, 1928–1935.

2 S. Feng, J. Lu, L. Luo, G. Qian, J. Chen, H. S. Abbo, S. J. J. Titinchi and S. Yin, Enhancement of oxygen reduction activity and stability via introducing acid-resistant refractory Mo and regulating the near-surface Pt content, *J. Energy Chem.*, 2020, **51**, 246–252.

3 S. Zhang, S. Liu, J. Huang, H. Zhou, X. Liu, P. Tan, H. Chen, Y. Liang and J. Pan, Microbial synthesis of N, P co-doped carbon supported PtCu catalysts for oxygen reduction reaction, *J. Energy Chem.*, 2023, **84**, 486–495.

4 C. T. Dameron, R. N. Reese, R. K. Mehra, A. R. Kortan, P. J. Carroll, M. L. Steigerwald, L. E. Brus, D. R. Winge, C. T. Dameron, *et al.*, Biosynthesis of cadmium sulphide quantum semiconductor crystallites, *Nature*, 1989, **338**, 596–597.

5 P. Mukherjee, A. Ahmad, D. Mandal, S. Senapati, S. R. Sainkar, M. I. Khan, R. Parishcha, P. V. Ajaykumar, M. Alam, R. Kumar and M. Sastry, Fungus-Mediated Synthesis of Silver Nanoparticles and Their Immobilization in the Mycelial Matrix: A Novel Biological Approach to Nanoparticle Synthesis, *Nano Lett.*, 2001, **1**, 515–519.

6 S. A. Dahoumane, M. Mechouet, K. Wijesekera, C. D. M. Filipe, C. Sicard, D. A. Bazylinski and C. Jeffryes, Algae-mediated biosynthesis of inorganic nanomaterials as a promising route in nanobiotechnology – a review, *Green Chem.*, 2017, **19**, 552–587.

7 J. Yang, P. Ju, X. Dong, J. Duan, H. Xiao, X. Tang, X. Zhai and B. Hou, Green synthesis of functional metallic nanoparticles by dissimilatory metal-reducing bacteria "Shewanella": a comprehensive review, *J. Mater. Sci. Technol.*, 2023, **158**, 63–76.

8 S. Zhang, H. Zhou, H. Liao, P. Tan, W. Tian and J. Pan, Microbial synthesis of efficient palladium electrocatalyst with high loadings for oxygen reduction reaction in acidic medium, *J. Colloid Interface Sci.*, 2022, **611**, 161–171.

9 Q. Lv, B. Zhang, X. Xing, Y. Zhao, R. Cai, W. Wang and Q. Gu, Biosynthesis of copper nanoparticles using Shewanella loihica PV-4 with antibacterial activity: novel approach and mechanisms investigation, *J. Hazard. Mater.*, 2018, **347**, 141–149.

11 Q. Li, S. Zhang, W. Xuan, H. Zhou, W. Tian, X. Deng, J. Huang, Z. Xie, F. Liu, X. Liu and Y. Liang, Microbial synthesis of highly dispersed nano-Pd electrocatalyst for oxygen reduction reaction, *Int. J. Hydrogen Energy*, 2021, **46**, 26886–26896.

12 L. Zhang, X. Huang, G. Fu and Z. Zhang, Aerobic electrotrophic denitrification coupled with biologically induced phosphate precipitation for nitrogen and phosphorus removal from high-salinity wastewater: Performance, mechanism, and microbial community, *Bioresour. Technol.*, 2023, **372**, 128696.

13 H. Li, S. Dai, Y. Wu, Q. Dong, H. Zhu, A. Hu, J.-P. Chou and T.-Y. Chen, Ir-trimer anchored on the Co-supported Pd nanocrystals opens the ultra-efficient channel on oxygen reduction reaction, *Appl. Surf. Sci.*, 2023, **622**, 156857.

14 X. Wu, C. Ni, J. Man, X. Shen, S. Cui and X. Chen, A strategy to promote the ORR electrocatalytic activity by the novel engineering bunched three-dimensional Pd-Cu alloy aerogel, *Chem. Eng. J.*, 2023, **454**, 140293.

15 X. Wang, L. Guo, Z. Xie, X. Peng, X. Yu, X. Yang, Z. Lu, X. Zhang and L. Li, Coordination environment engineering of graphene-supported single/dual-Pd-site catalysts improves the electrocatalytic ORR activity, *Appl. Surf. Sci.*, 2022, **606**, 154749.